Static and Cyclic Triaxial Testing of Ballast and Subballast

ARTICLE *in* JOURNAL OF GEOTECHNICAL AND GEOENVIRONMENTAL ENGINEERING · JUNE 2005

Impact Factor: 1.6 · DOI: 10.1061/(ASCE)1090-0241(2005)131:6(771)

3 AUTHORS, INCLUDING:

Akke Suiker
Technische Universiteit Eindhoven
58 PUBLICATIONS **1,240** CITATIONS

Static and Cyclic Triaxial Testing of Ballast and Subballast

Akke S. J. Suiker[1]; Ernest T. Selig[2]; and Raymond Frenkel[3]

Abstract: This paper discusses the triaxial testing of a ballast material and a subballast material, which are noncohesive, granular materials typically used for construction of a railway track substructure. Both static and cyclic triaxial tests were conducted. The cyclic triaxial tests simulated the behavior of these railway substructure materials under a large number of passing train wheels. The purpose of the static tests was to a priori identify the maximum stress level that could be applied in the cyclic tests, and to assess the strength and stiffness increase produced during the cyclic loading process. In order to accurately monitor the circumferential displacement during the static and cyclic tests, a new measuring device was developed. The experimental setup, the test procedure, and the test results are treated for the ballast and subballast materials. It is found that under cyclic loading the granular materials reveal a strong tendency to compact, even if the applied stress level is close to the static failure strength of the material. This compaction behavior generally causes a (significant) increase of the material strength and stiffness.

DOI: 10.1061/(ASCE)1090-0241(2005)131:6(771)

CE Database subject headings: Cyclic tests; Triaxial tests; Static tests; Railroad ballast; Railroad tracks.

Introduction

The geometry of railway tracks requires a specific level and alignment in order to have acceptable ride quality and to meet safety standards. For ballasted railway tracks, the level and alignment of the track structure strongly rely on the mechanical characteristics of the granular substructure, which is composed of a ballast layer, a subballast layer, and subgrade layers. In fact, the generation of progressive permanent deformations in the granular substructure is the main factor in the emergence of track irregularities of a medium to long wavelength, i.e., wavelengths between 3 and 50 m (Esveld 1989). When track irregularities exceed allowable limits, either traffic speed restrictions have to be prescribed, or maintenance has to be performed to recover a tolerable track level and alignment (Esveld 1989; Selig and Waters 1994).

Most track maintenance is carried out mechanically. The two available maintenance procedures applied to correct track irregularities of a medium to long wavelength are "tamping" and "stoneblowing" (Selig and Waters 1994). In the case of tamping, the ties are lifted separately to a prescribed level, after which a tamping unit of steel tools vibrates and squeezes the underlying ballast particles to fill the voids beneath the lifted ties. The tamping procedure is repeated at each tie in the segment of track needing smoothing. A disadvantage of tamping is that it loosens the ballast and also breaks the particles (Esveld 1989; Selig and Waters 1994). The alternative to tamping is stoneblowing, where, instead of squeezing the ballast particles, a predetermined quantity of small stones is pneumatically injected into the void created by the lifted tie. In contrast to tamping, stoneblowing thus causes the original ballast layer to be minimally disturbed. This may result in an improved postmaintenance performance if the size and type of the stone and the thickness of the injected layer are chosen adequately (Esveld 1989; Anderson and Key 2000).

For optimizing maintenance operations, prediction of maintenance periods, and detailed understanding of the effect of maintenance procedures, insight is required into the mechanical behavior of ballast and subballast materials under static and cyclic loading conditions. Previous laboratory testing has yielded much knowledge in this research area (Brown 1974; Raymond and Davies 1978; Alva-Hurtado 1980; Stewart 1982; Selig and Waters 1994; Indraratna et al. 1998; Anderson and Key 2000), though there are still issues that need to be studied in more detail. For example, for the (numerical) modeling of track deterioration (Suiker 2002; Suiker and de Borst 2003), it is important to identify appropriate stress and strain measures that adequately represent the substructure material behavior under cyclic loading conditions. Also, further examination is necessary of the effect of the cyclic loading process on the material stiffness, the failure strength, and the deformation characteristics of various ballast and subballast materials. Accordingly, a large-scale laboratory testing program was performed in which static and cyclic triaxial tests on a ballast material and a subballast material were performed at stress levels relevant for railway structures (Suiker 1999). The tests were carried out at a constant confining pressure, which simulates the mean pressure due to geostatic stresses in a railway structure. In the cyclic triaxial tests, each vertically applied load cycle was returned to full unloading which is assumed to mimic the effect of a passing train wheel. Both the reversible and irreversible components of the vertical displacement and the circumferential displacement were measured. For this purpose, a new type of circumferential displacement device was developed.

[1]Assistant Professor, Delft Univ. of Technology, Koiter Institute Delft/Faculty of Aerospace Engineering, P.O. Box 5058, NL-2600 GB Delft, The Netherlands.

[2]Emeritus Professor, Univ. of Massachusetts, Dept. of Civil and Environmental Engineering, 28, Marston Hall, Amherst, MA 01003.

[3]Graduate Research Assistant, Univ. of Massachusetts, Dept. of Civil and Environmental Engineering, 28, Marston Hall, Amherst, MA 01003.

Note. Discussion open until November 1, 2005. Separate discussions must be submitted for individual papers. To extend the closing date by one month, a written request must be filed with the ASCE Managing Editor. The manuscript for this paper was submitted for review and possible publication on November 20, 2002; approved on November 1, 2004. This paper is part of the ***Journal of Geotechnical and Geoenvironmental Engineering***, Vol. 131, No. 6, June 1, 2005. ©ASCE, ISSN 1090-0241/2005/6-771–782/$25.00.

This paper describes the experimental setup, the test procedure, and the test results for the specific ballast material and subballast material examined.

Materials and Apparatus

Material Description

The grain-size distribution of the subballast and ballast materials have been depicted in Fig. 1. According to the ASTM D2488 (1997), the subballast is designated a well-graded sand with gravel. The ballast is designated a uniformly graded gravel, with particles consisting of crushed basalt, which is a dark-colored igneous rock. Ballast is produced by crushing rock and sieving it to get the desired particle sizes. The ballast fulfills the requirement of a gradation No. 4, as specified in the AREMA Manual for Railway Engineering (AREMA 2002). For assigning in the development and validation of track geometry deterioration models (Suiker 2002; Suiker and de Borst 2003), the characteristics of the ballast and subballast materials were taken similar to those of the in situ testtrack in Pueblo, Colo. (Selig et al. 1981), so that the test-track performance data could be used. The compaction characteristics of the subballast material were determined as described in ASTM D698, procedure *C* (1997). This resulted in an average maximal dry unit weight of the subballast samples of $\gamma_{dry,max}=19.2$ kN/m^3 at an optimum moisture content of 5.5%.

Experimental Setup

The cylindrical material specimen used in the subballast triaxial tests had a nominal height of $H=357$ mm and a nominal diameter of $D=153$ mm, corresponding to an aspect ratio of $H/D=2.33$. According to Fig. 1, the largest grain size in the subballast material is$d=20$ mm, yielding a specimen diameter to grain size ratio of $D/d\approx 8$. The triaxial load apparatus used for the ballast testing was identical to the load apparatus used for the subballast testing. However, since the average particle size of a ballast gradation is larger than that of a subballast gradation, the size of the triaxial load apparatus for the ballast tests is bigger in order to reduce the influence of size effects. The nominal height of the cylindrical ballast specimen was equal to $H=645$ mm and the nominal diameter was equal to $D=254$ mm yielding an aspect ratio of $H/D=2.53$. The largest grain size in the uniformly graded ballast material is $d=38$ mm, see Fig. 1, corresponding to a specimen diameter to grain size ratio of $D/d\approx 7$.

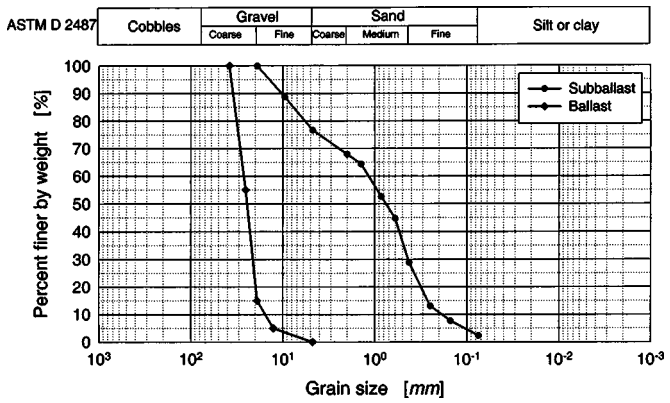

Fig. 1. Grain-size distribution of ballast and subballast materials

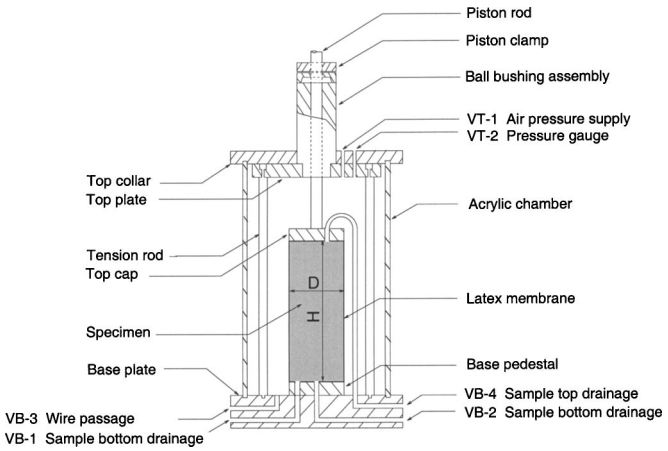

Fig. 2. Components of triaxial load apparatus

The triaxial apparatus used in the tests is illustrated in Fig. 2. The subballast specimens tested with this apparatus were compacted toward 95–97% of $\gamma_{dry,max}$. This occurred by preparing samples at a moisture content of 5.5%, followed by placing and compacting nine material layers of equal thickness. The compaction procedure occurred by striking the individual layers 20 times with a standard Proctor hammer. Because a ballast consists of large regular particles with large void spaces, the material has a high water permeability. The behavior of a ballast with this gradation is therefore not sensitive to water content. The preparation of a dry ballast specimen occurred by placing and compacting eight layers of equal thickness. Each layer was tamped 40 strokes with a steel rod. The method of layered compaction is also applied during in situ construction of ballast and subballast layers (Selig and Waters 1994); this method inherently causes the material density to be nonuniform over the structural height, since the bottom layers receive more compaction energy than the top layers.

The subballast specimen was enclosed by a double-latex membrane with a total thickness of 0.6 mm. The ballast specimen was enclosed by a latex membrane of 0.76 mm thickness that was manually cut from a roll and subsequently glued together. The total thickness of the membrane for the ballast specimen is somewhat higher than for the subballast specimen, in order to avoid membrane puncturing by the sharp edges of the ballast particles. The membranes had an air-tight connection with the top cap and the base pedestal, by means of neoprene *O* rings. The base pedestal facilitated the connection of the compaction mould necessary for constructing the specimen. The top and bottom of the specimen were treated with grease in order to reduce the friction with the top cap and the base pedestal, respectively.

During the fabrication of the specimen, the membrane was held against the wall of the compaction mould by applying a vacuum. After the specimen was built, the top cap was attached and the compaction mould was removed while a temporary internal vacuum was created to keep the specimen standing. For the subballast specimen, the second membrane was placed to provide an air-tight lateral boundary. Subsequently, the top plate, the acrylic chamber, and the top collar were installed. A constant confining air pressure was applied to the acrylic chamber through Valve VT-1. The air pressure was measured via a pressure gauge that entered the acrylic chamber through Valve VT-2. The regulation of the pressure was provided by means of an external pressure control system. The Valves VB-1 and VB-2 controlled the

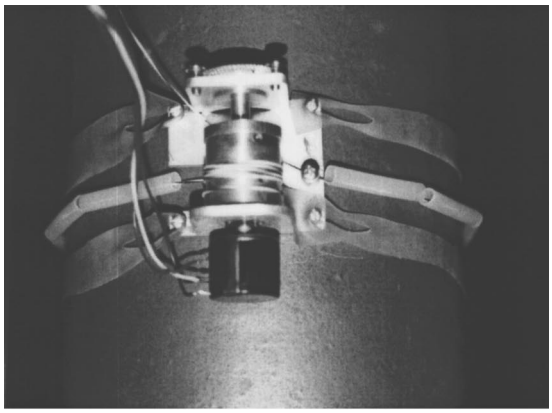

(a)

(b)

Fig. 3. Specimen and displacement measuring device: (a) circumferential displacement device attached to a subballast specimen, and (b) three circumferential displacement devices attached to a ballast specimen

drainage at the bottom of the specimen, whereas Valve VB-4 controlled the drainage at the top of the specimen. During the experiments, the drainage from the specimen to atmospheric pressure occurred freely; i.e., the back pressure inside the specimen equals the atmospheric pressure. Valve VB-3 provided access for the electric wires of the device that measured the circumferential displacement of the specimen.

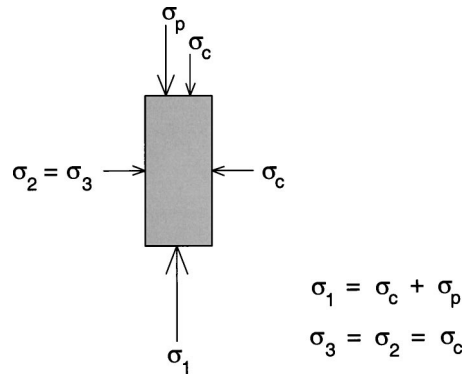

Fig. 4. Axisymmetric stress state in a conventional triaxial test

For the subballast specimen, the circumferential displacement device was mounted at the midheight of the specimen. The device is a newly developed concept comprising a Teflon-coated multistranded steel cable of 1 mm diameter, which encloses the specimen circumference and is wound up by a small aluminum cylinder of 24 mm diameter, see Fig. 3(a). The cylinder is mounted on the shaft of a three-turn potentiometer, which registers the change in length of the specimen circumference. The relative resolution of the potentiometer is 0.044%, which results in a measuring inaccuracy of 0.1 mm over a total cable length of 225 mm. For minimizing the friction around the cable, the cable is surrounded by pieces of Teflon tubing, thus providing the cable with a Teflon-to-Teflon contact. The cable needs to be kept under a small tension in order to maintain the contact between the Teflon tubing and the specimen. The tension is applied by means of a rotational spring that is placed inside the aluminum cylinder. The cable tension can be regulated through a turning wheel on top of the device, which is connected to the spring. The device is mounted onto a small aluminum plate, which is attached to the sample by means of latex bands that were cut from a (previously used) membrane. The circumferential displacement device can be made with relatively low manufacturing costs, it has a low weight, a relatively small size, and can be easily incorporated into a triaxial apparatus that does not have a circumferential (or radial) displacement device as a standard outfit. More technical information about the circumferential displacement device is given in Frenkel (2000). For the ballast specimen, the relatively large specimen height H allowed for installing three (instead of one) circumferential displacement devices, which were attached at $H/3$, $H/2$, and $2H/3$, see Fig. 3(b).

The specimen deformation in vertical direction was measured by an external displacement transducer that was clamped onto the piston rod. The displacement transducer touched the top collar and thus registered the sample movement relative to the top collar. A data acquisition program was developed to store the measured vertical displacement, the circumferential displacement, the vertical load, and the confining pressure.

Triaxial Testing on Subballast

Stress and Strain Definitions

The axisymmetric stress conditions applied to the cylindrical specimen are defined in Fig. 4. The shear stresses in the 1- and 3-directions (=2-direction) are supposed to be zero, so that the normal stresses in these directions correspond to the principal

stresses. The principal stress, σ_1, results from the summation of the confining pressure, σ_c, and the stress applied via the loading piston, σ_p, while the principal stress, σ_3, is equal to the confining pressure. The friction at the bearing that supports the loading shaft is regarded as minimal, and thus neglected in the computation of the principal stress σ_1.

Instead of using the principal stresses for describing the material response, in the field of granular mechanics a deviatoric stress invariant, q, and a hydrostatic stress invariant, p, are often employed (see for example, Vardoulakis and Sulem 1995). This is, because the stress ratio $-q/p$ is an appropriate measure for describing frictional failure of a granular material under three-dimensional stress conditions. In their general form, these stress invariants are given by

$$q = \sqrt{\tfrac{3}{2} s_{ij} s_{ij}}$$

$$p = \tfrac{1}{3}\sigma_{kk} \tag{1}$$

where s_{ij}=deviatoric stress tensor, according to

$$s_{ij} = \sigma_{ij} - p\delta_{ij} \tag{2}$$

where δ_{ij}=Kronecker delta symbol. The energy conjugates of the stress invariants given in Eq. (1) are the deviatoric strain invariant κ and the volumetric strain invariant ε_{vol}, respectively, as represented by

$$\kappa = \sqrt{\tfrac{2}{3} \gamma_{ij} \gamma_{ij}}$$

$$\varepsilon_{\text{vol}} = \varepsilon_{kk} \tag{3}$$

where γ_{ij}=deviatoric strain tensor

$$\gamma_{ij} = \varepsilon_{ij} - \tfrac{1}{3}\varepsilon_{\text{vol}}\delta_{ij} \tag{4}$$

For the axisymmetric configuration depicted in Fig. 4, the stress invariants, Eq. (1), simplify to

$$q = |\sigma_1 - \sigma_3| = \sigma_p$$

$$p = \tfrac{1}{3}(\sigma_1 + 2\sigma_3) = \sigma_c + \tfrac{1}{3}\sigma_p \tag{5}$$

whereas the strain invariants, Eq. (3), reduce to

$$\kappa = \tfrac{2}{3}|\varepsilon_1 - \varepsilon_3|$$

$$\varepsilon_{\text{vol}} = \varepsilon_1 + 2\varepsilon_3 \tag{6}$$

where ε_1 and ε_3=principal strains, oriented in the axial and radial directions of the specimen, respectively. In the present paper, the solid mechanics sign convention is used, where tension and dilation are designated by a positive sign and compression and contraction are designated by a negative sign.

In the cyclic tests, the stress applied via the piston, σ_p, is composed of a small static part and a cyclic part: $\sigma_p = \sigma_{p,\text{stat}} + \sigma_{p,\text{cyc}}$. The static part is necessary for maintaining contact between the hydraulic load actuator and the specimen, which was achieved by application of a relatively small loading of 100 N. The cyclic part varied between zero and a specific fraction n of the static failure load $(-q/p)_{\text{stat,max}}$. Accordingly, n is denoted as the "relative cyclic stress," and can be expressed as

$$n = \frac{(-q/p)_{\text{cyc}}}{(-q/p)_{\text{stat,max}}} \tag{7}$$

where $(-q/p)_{\text{cyc}}$=stress amplitude for an individual load cycle.

Results from Static Tests

Static failure tests were performed to determine the maximum stress level that could be applied in the cyclic triaxial tests. After the static tests were finished, the cyclic tests were carried out. In the static tests, the specimen response was measured at three different (constant) confining pressures: $\sigma_c = -10.3$ kN/m^2, -41.3 kN/m^2, and -68.9 kN/m^2. The characteristics of each test have been summarized in Table 1. The initial dry unit weight of the subballast materials presented in Table 1 falls within the range of values of 17.0 kN/m^3 $< \gamma_{\text{dry}} <$ 18.7 kN/m^3, measured for the well-graded sandy subballast layer in the Colorado testtrack (Selig et al. 1981). This indicates that the compaction characteristics of the tested subballast are representative for subballast layers in situ. The last two characters of the test indication used in Table 1 are an abbreviation of the type of material tested, i.e., "sb" stands for subballast. The specimen response during the static tests was controlled by means of the displacement in the axial direction. Use of displacement-controlled tests made it possible to monitor unstable material behavior.

Fig. 5(a) depicts the measured normalized deviatoric stress $-q/p$ versus the deviatoric strain κ at the three selected confining pressures. The stress parameters relate to the specimen cross section in the actual deformation state (i.e., Cauchy stress). The strain values in Fig. 5(a) were not corrected for membrane penetration, since for relatively dry materials the error made by ignoring the membrane penetration is commonly small; e.g., Hjortnaes-Pedersen and Molenkamp (1982) reported a difference of 0.0003 (mm/mm) in deviatoric strain for triaxial test results with and without correction for membrane penetration. Since the sample has a moisture content of 5.5%, in principle, an apparent cohesion is generated as a result of suction of water. However, this effect is regarded as negligible. In Fig. 5(a), it can be observed that the deviatoric stress initially increases with increasing deviatoric strain until it reaches the peak strength. Apparently, for a higher confining pressure, the peak strength becomes lower and the strain corresponding to the peak strength becomes higher. The small deviation in peak strength is a typical consequence of the dependence of particle interlocking upon the confining pressure (Lambe and Whitman 1969); the interlocking of particles (and thus the peak strength) decreases as the confining pressure increases, since particles become polished at contact points and sharp corners are crushed.

All three curves in Fig. 5(a) show that in the postpeak regime, the stress reduces with increasing strain; this behavior is typical for *dense* granular materials and is commonly characterized as *strain softening* (see, for example, van der Giessen and de Borst 1998). The strain-softening process is concomitant with the generation of large deformations, which causes geometrically nonlinear effects to become important. In the present study, the assessed strain range is limited to about 5%, which more or less bounds the deformation range relevant for the cyclic behavior of railway sub-

Table 1. Characteristics of Static Triaxial Tests on Subballast Material

Test	Confining pressure σ_c (kN/m^2)	Wet unit weight γ_{wet} (kN/m^3)	Dry unit weight γ_{dry} (kN/m^3)	Proctor density[a] (%)
Stat.1sb	−10.3	19.0	18.1	94.3
Stat.2sb	−41.3	19.3	18.5	96.4
Stat.3sb	−68.9	19.3	18.3	95.3

[a]Note: sb=subballast. Dry unit weight expressed as a precentage of the ASTM D698 maximum dry unit weight.

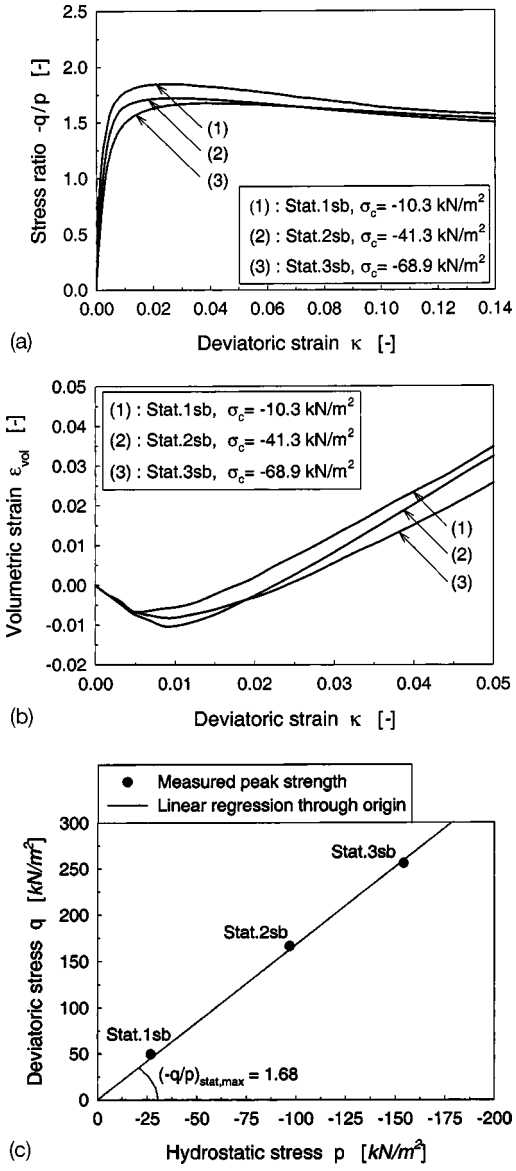

Fig. 5. Static response of subballast material: (a) variation of stress ratio $-q/p$ with the total deviatoric strain κ for various confining pressures σ_c; (b) variation of total volumetric strain ε_{vol} with total deviatoric strain κ for various confining pressures σ_c; and (c) comparison of measured values of peak strength in the $p-q$ plane with linear regression line

structure materials (Selig and Waters 1994). In addition, a strain value of 5% is considered to be the limit of applicability of the small strain theory [used in Eqs. (3), (4), and (6)].

In Fig. 5(b), the deviatoric strain measured in the 0–5% strain range is depicted versus the volumetric strain. The strain parameters have been computed by using Eq. (6), in which the principal strains ε_1 and ε_3 have been derived from the measured vertical displacement and circumferential displacement, respectively. It is seen that the volumetric strain is initially compressive ($\dot{\varepsilon}_{vol}<0$) and becomes dilative ($\dot{\varepsilon}_{vol}>0$) at increasing deviatoric strain. For an increasing confining pressure, the amount of dilation produced during failure decreases; this is a commonly observed feature in the triaxial testing of dense noncohesive granular materials (Lee and Seed 1967; Lambe and Whitman, 1969; Raymond and Davies 1978; Wood 1990). The minor wrinkles appearing at the onset of the response were caused by a local temporarily circumferential stiffening, resulting from the bending resistance of the pieces of Teflon tubing surrounding the Teflon-coated steel cable. For subsequent tests, this problem was solved by cutting the Teflon tubing into smaller pieces.

The peak strength of noncohesive granular materials in triaxial compression is often interpreted by means of a Mohr–Coulomb criterion (Lambe and Whitman 1969; Wood 1990; Vardoulakis and Sulem 1995). The Mohr–Coulomb criterion is a purely frictional criterion, where the deviatoric strength increases linearly with the hydrostatic pressure; hence deviations in peak strength as a result of the effect of confining pressure upon interlocking are left out of consideration. Fig. 5(c) shows the result of a linear regression that has been applied to the peak strengths measured at the three selected confining pressures. The regression line has been constructed by requiring that it passes the origin, thus characterizing a noncohesive material. The slope of the regression line relates to a peak strength of $(-q/p)_{stat,max}=1.68$. In agreement with the Mohr–Coulomb criterion, this value corresponds to a friction angle $\phi_{stat,max}=41°$.

Results from Cyclic Tests

After the above-mentioned static tests were completed, cyclic tests were carried out at two selected (constant) confining pressures: $\sigma_c=-41.3$ kN/m^2 and $\sigma_c=-68.9$ kN/m^2. The specimen response was measured during one million load cycles. At both confining pressures, four different cyclic stress levels were considered, resulting in the total of eight tests. The cyclic loading was applied in the axial direction of the specimen, where each load cycle returned to full unloading, as representative of a passing train wheel. The constant confining pressure mimics the mean pressure due to geostatic stresses in a railway track. The cyclic

Table 2. Characteristics of One Million Load Cycle Tests on Subballast Material

Test	Confining pressure σ_c (kN/m^2)	Relative cyclic stress n (−)	Wet unit weight γ_{wet} (kN/m^3)	Dry unit weight γ_{dry} (kN/m^3)	Proctor density[a] (%)
Cyc.1sb	−41.3	0.495	19.2	18.5	96.4
Cyc.2sb	−41.3	0.845	19.3	18.4	95.8
Cyc.3sb	−41.3	0.960	19.1	18.4	95.8
Cyc.4sb	−41.3	0.995	19.3	18.4	95.8
Cyc.5sb	−68.9	0.545	19.3	18.5	96.4
Cyc.6sb	−68.9	0.821	19.4	18.6	96.9
Cyc.7sb	−68.9	0.950	19.4	18.6	96.9
Cyc.8sb	−68.9	0.975	19.3	18.5	96.4

[a]Dry unit weight expressed as a percentage of the ASTM D698 maximum dry unit weight.

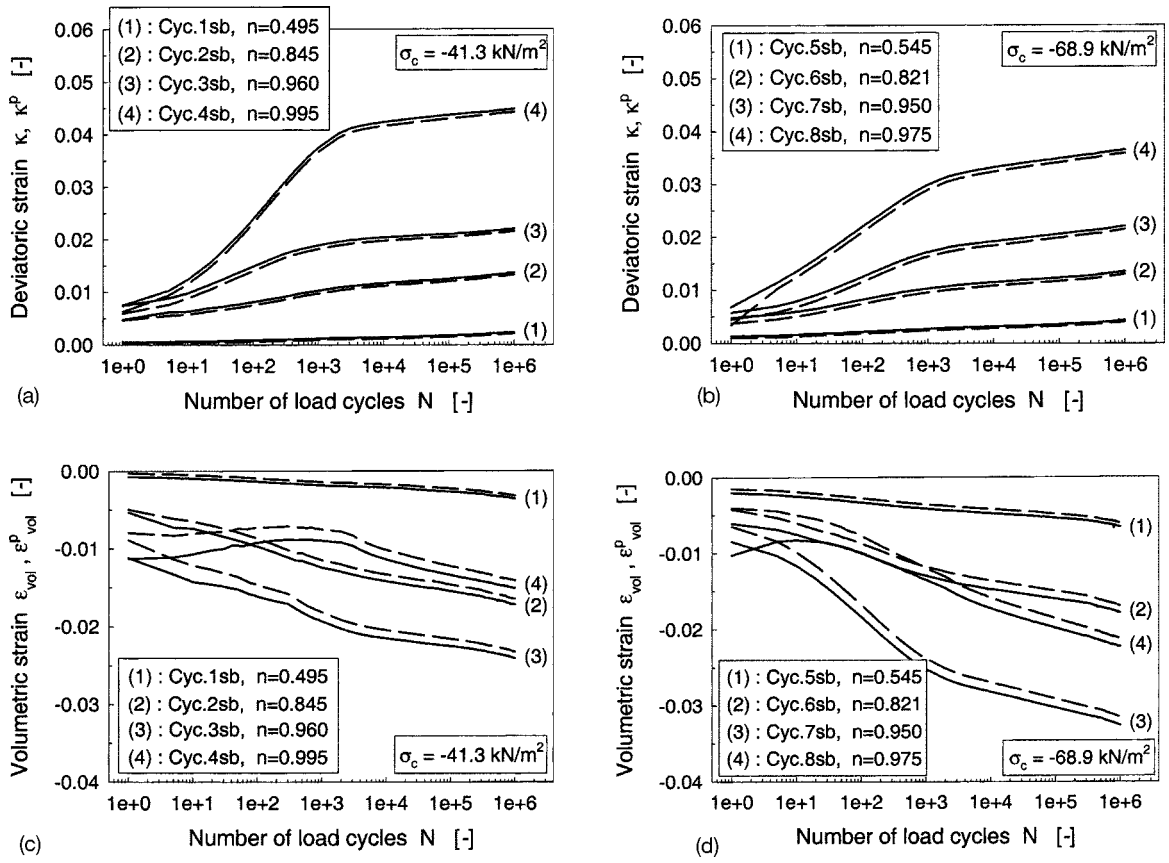

Fig. 6. Cyclic response of subballast material for various stress levels n: (a) increase of total deviatoric strain κ (solid line) and permanent deviatoric strain κ^p (dashed line) with load cycles N, for a confining pressure $\sigma_c = -41.3$ kN/m^2; (b) increase of total deviatoric strain κ (solid line) and permanent deviatoric strain κ^p (dashed line) with load cycles N, for a confining pressure $\sigma_c = -68.9$ kN/m^2; (c) variation of total volumetric strain ε_{vol} (solid line) and permanent volumetric strain ε^p_{vol} (dashed line) with load cycles N, for a confining pressure $\sigma_c = 41.3$ kN/m^2; and (d) variation of total volumetric strain ε_{vol} (solid line) and permanent volumetric strain ε^p_{vol} (dashed line) with load cycles N, for a confining pressure $\sigma_c = -68.9$ kN/m^2

tests were performed in a load-controlled fashion, using a periodic positive full-sine signal with a frequency of 5 Hz. A comparison with preliminary tests conducted at lower frequencies revealed that at 5 Hz, the mass inertia effects of the specimen were negligibly small so that the material response may be characterized as "quasi-static." The data storage occurred after prescribed loading intervals, where each data point corresponds to a specific load cycle. During such a load cycle, the displacements in the axial and radial directions were read 100 times, where the maximum value over the total amount of readings was assumed to be equal to the incremental total displacement and the value at the end of the load cycle was considered to represent the incremental permanent displacement. The conditions for the cyclic triaxial tests are listed in Table 2.

Figs. 6(a and b) show the measured deviatoric strain κ versus the logarithm of the number of load cycles N for the two confining pressures considered. The curves consist of two lines, the solid line reflecting the total deformation and the dashed line reflecting the permanent deformation. The difference between the two lines equals the elastic deformation. It is evident that an increasing cyclic stress level n causes the total deviatoric deformation to increase, where the growth of the deviatoric deformation is mainly governed by the permanent deformation component. The response characteristics are about the same for the confining pressures considered, indicating that the cyclic development of the deviatoric strain may be objectively characterized by the relative cyclic stress n, or analogously, by the cyclic stress level $(-q/p)_{cyc}$.

In Figs. 6(c and d), the cyclic evolution of the volumetric strain is plotted for the two selected confining pressures. Again, the solid line represents the total deformation and the dashed line represents the permanent deformation. During the first 100 to 1,000 load cycles, both lines grow steadily toward each other, implying that the elastic volumetric deformation decreases and the granular material becomes stiffer. In the literature, this phase is regularly referred to as the "conditioning phase" (Brown 1974; Galjaard et al. 1996). During the subsequent loading stage, the elastic deformation remains approximately constant, where, for an individual load cycle, the elastic strain component is much greater than the permanent strain component. This implies that considerable material compaction has taken place. The tests carried out at a confining pressure $\sigma_c = -68.9$ kN/m^2, in general, display a stronger compaction than those carried out at $\sigma_c = -41.3$ kN/m^2; this effect was also observed for the static tests, see subsection entitled, "*Results from Static Tests*."

Figs. 6(c and d) illustrate that, up to a stress level of $n \approx 0.96$, a higher cyclic stress causes more compaction. However, for cyclic stress levels close to the static failure strength, $0.96 < n < 1$, the specimen initially shows a dilative behavior that is inherent to the high stress level, which proceeds into compaction

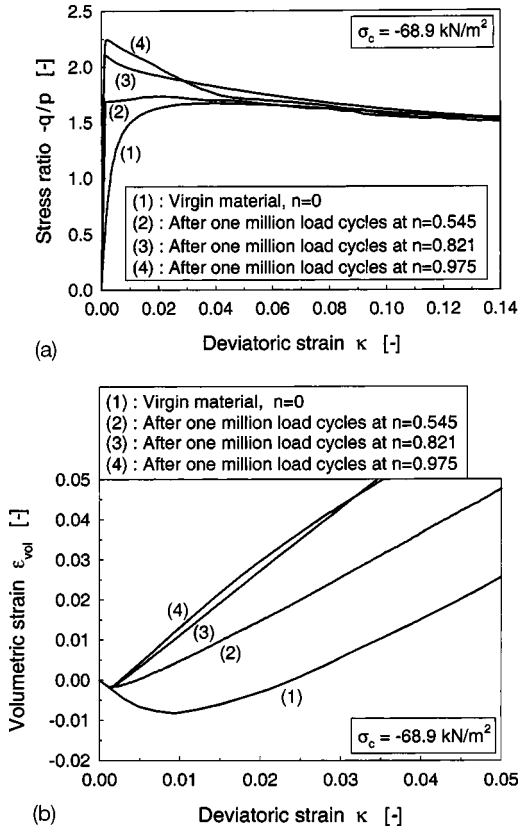

Fig. 7. Static response of subballast material after preloading at various cyclic stress levels n: (a) variation of stress ratio $-q/p$ with total deviatoric strain κ, where the confining pressure $\sigma_c = -68.9$ kN/m^2, and (b) variation of total volumetric strain ε_{vol} with total deviatoric strain κ, where the confining pressure $\sigma_c = -68.9$ kN/m^2

as a result of the increasing number of load cycles. In other words, the high stress level and the load cycles have an opposite effect on the volumetric deformation characteristics. Note that the compaction rate $d\varepsilon_{vol}^p/dN$ becomes consistently higher for a higher cyclic stress level after more than 2,000 load cycles have occurred.

It can be expected that the cyclic loading process alters the strength and stiffness properties of the granular specimens. To obtain more insight into this phenomenon, the specimens were brought to static failure after the cyclic loading tests were finished. The results of these so-called "postcyclic failure tests" are discussed below.

Static Failure after Cyclic Loading

In Fig. 7(a), the stress-strain curves during postcyclic failure are plotted together with the static failure curve of the virgin material (i.e., Test *Stat.3sb*, see Table 1). In fact, the latter test relates to a relative cyclic stress level $n=0$. The confining pressure of the tests equals $\sigma_c = -68.9$ kN/m^2, and the deviatoric strain κ is measured from the onset of static loading (i.e., the deviatoric strain was reset to zero after the cyclic loading process finished). It can be seen that a priori subjecting the material to cyclic loading may elevate the static peak strength significantly. Recall that Figs. 6(c and d) showed that the material density obtained through the cyclic loading process generally is higher for a higher cyclic stress level, but that at very high cyclic stress levels, i.e., $n=0.975$, the total compaction obtained at the end of the cyclic loading process tends to decrease for an increasing cyclic stress level. Hence, the relatively strong particle structure generated at $n=0.975$ relates to a small total change in specimen density, implying that considerable particle rearrangement has taken place.

After the application of 1,000,000 load cycles at $n=0.975$, the postcyclic peak strength has become 34% higher than the peak strength of the virgin material. The Mohr–Coulomb friction angles corresponding to the peak strengths are computed as: $\phi_{stat,max}=41°$ ($n=0$), $\phi_{stat,max}=43°$ ($n=0.545$), $\phi_{stat,max}=51°$ ($n=0.821$), and $\phi_{stat,max}=55°$ ($n=0.975$). Although not clearly observable from Fig. 7(a), the strain corresponding to the post-cyclic peak strength decreases when the cyclic stress level increases, implying that there will be less "warning" for the occurrence of postcyclic failure.

Apart from increasing the peak strength, the cyclic loading process also increases the material stiffness, as embodied by the increase of the initial slope of the stress-strain curves. For the virgin material ($n=0$), the secant shear stiffness for a stress ratio, $-q/p=1.0$, equals $\mu^s_{-q/p=1.0}=11$ MPa. In contrast, after the application of 1,000,000 load cycles at either $n=0.545$, $n=0.821$, or $n=0.975$, the secant shear stiffness has become approximately equal to $\mu^s_{-q/p=1.0}\approx 80$ MPa, reflecting a stiffness increase of a factor of 7.

In the softening branch of the stress-strain response, the individual curves in Fig. 7(a) grow towards each other, indicating that the shear strength then becomes independent of the initial compaction level of the granular specimen. In addition, for an increased cyclic stress level, the postpeak drop off in strength becomes more pronounced. This feature is related to the observation that the specimen fails more locally if the stress level during the cyclic loading process is higher; i.e., for the virgin material, $n=0$, a bulging-type failure mode was observed, whereas the material subjected to a high cyclic stress, $n=0.975$, failed statically under the development of a local shear band.

The deformation characteristics for the postcyclic failure tests have been plotted in Fig. 7(b). It can be seen that the transition from material compaction into material dilation occurs faster if the stress level during the cyclic loading stage is higher. Because for dense granular materials the onset of dilation generally is a precursor to frictional failure, a faster transition into dilation relates to a smaller deformation necessary for reaching (postcyclic) failure.

Test Repeatability and Response to 5,000,000 Load Cycles

The cyclic loading tests discussed above were ended when the number of load cycles exceeded 1,000,000. The deformation rate measured during these tests generally decreased at an increased number of load cycles. This tendency can be expected to continue when the number of load cycles becomes larger than 1,000,000. It is important to verify this, since in railway practice a maintenance period may span more train passages than the equivalent of 1,000,000 load cycles. Hence, the number of load cycles in a cyclic test was increased to 5,000,000. Because the performance of a 5,000,000 load cycles test is time consuming, only one test was carried out.

The conditions for the 5,000,000 load cycles test are presented in Table 3. Note that the cyclic stress level applied in this test is close to the failure strength of the virgin material. Since the characteristics of Test *Cyc.9sb* (see Table 3) closely resemble those of test *Cyc.3sb* (see Table 2), both tests are compared in order to

Table 3. Characteristics of Five Million Load Cycle Test on Subballast Material

Test	Confining pressure σ_c (kN/m^2)	Relative cyclic stress n (−)	Wet unit weight γ_{wet} (kN/m^3)	Dry unit weight γ_{dry} (kN/m^3)	Proctor density[a] (%)
Cyc.9sb	−41.3	0.98	19.3	18.6	96.9

[a]Dry unit weight expressed as a precentage of the ASTM D698 maximum dry unit weight.

check the test repeatability. Fig. 8(a) depicts the cyclic evolution of the deviatoric strain for the two tests, whereas Fig. 8(b) depicts the cyclic evolution of the volumetric strain. The trend of the deformation sketched in these figures is qualitatively the same for both tests. In a quantitative sense there are some differences, in particular with respect to the evolution of the volumetric strain. These discrepancies are due to small dissimilarities in the specimen density and the applied cyclic loading level, see Tables 2 and 3; because the cyclic stress level is close to the static failure strength, a small variation in stress may already cause a substantial variation in deformation.

For Test *Cyc.9sb*, the deformation generated between 1,000,000 and 5,000,000 load cycles is obviously very small compared to the deformation generated over the complete loading period. The deformation rate progressively decreases, even though the cyclic stress level is very close to the static failure level of the virgin material.

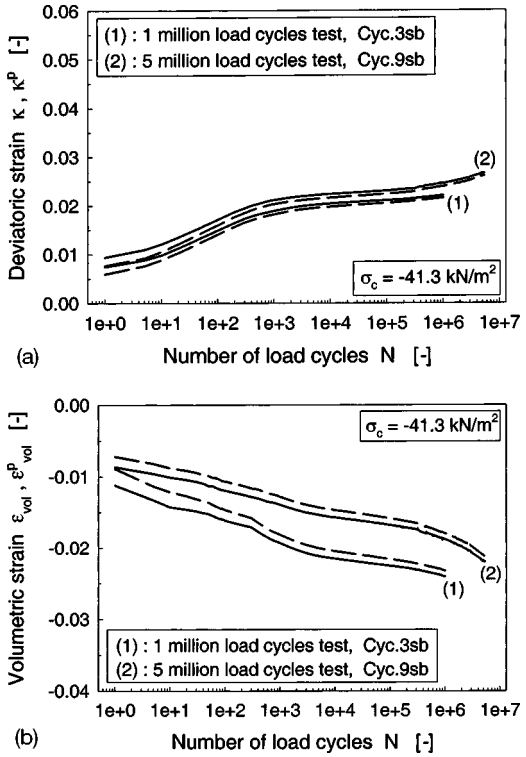

Fig. 8. Cyclic response of subballast material. Representation of test repeatability and response characteristics up to 5,000,000 load cycles. (a) Increase of total deviatoric strain κ (solid line) and permanent deviatoric strain κ^p (dashed line) with load cycles N. The confining pressure $\sigma_c = -41.3$ kN/m^2. (b) Decrease of total volumetric strain ε_{vol} (solid line) and permanent volumetric strain ε_{vol}^p (dashed line) with load cycles N. The confining pressure $\sigma_c = -41.3$ kN/m^2.

Triaxial Testing of Ballast

Results from Static Tests

The properties of the static ballast tests are collected in Table 4. The initial dry unit weight of the ballast material for each test falls within the range of values, $16.1\ \text{kN/m}^3 < \gamma_{dry} < 17.6\ \text{kN/m}^3$, measured for the traprock ballast layer in the Colorado testtrack (Selig et al. 1981). This implies that the compaction characteristics of the tested ballast are representative for a traprock ballast layer in situ. The three confining pressures that were used in the ballast testing are equal to those used in the subballast testing. The static tests were carried out in a displacement-controlled fashion. The stress-strain curve measured at each confining pressure has been plotted in Figs. 9(a–c). Each figure consists of three curves, corresponding to the circumferential displacement measurements at $H/3$, $H/2$, and $2H/3$ [see Fig. 3(b)]. Apparently, the three stress-strain curves in each figure are nearly identical. The small spikes emerging in the response are due to stick-slip events between individual ballast particles. These local instabilities are registered at the specimen level because the ratio between the average ballast particle size and the specimen size is relatively large.

In contrast with the subballast material, material softening is not observed for the ballast material. The absence of material softening can be ascribed to the relatively *loose* particle structure of the ballast specimens. The loose arrangement of ballast particles is caused by the uniform character of the particle size distribution, see Fig. 1; uniformly graded materials are less susceptible to compaction than broadly graded materials, in which smaller particles are forced inside the spaces created by bigger particles. Due to this effect, the dry unit weight of the ballast specimens is lower than that of the subballast specimens, see Tables 1 and 4.

In Fig. 9(d) the peak strengths of the three stress-strain responses have been plotted in the $p-q$ plane. As for the subballast, a Mohr–Coulomb criterion that passes the origin in the $p-q$ plane gives a reasonable approximation of the frictional failure level. The peak strength, $(-q/p)_{stat,max} = 1.98$, is somewhat higher than that of the subballast material, and relates to a Mohr–Coulomb friction angle of $\phi_{stat,max} = 48°$.

In Figs. 10(a–c), the quasi-static deformation characteristics measured at the selected confining pressures are depicted. The three figures actually reveal an identical trend; initially the material displays some compaction, which evolves relatively fast into

Table 4. Characteristics of Static Triaxial Tests on Ballast Material

Test	Confining pressure σ_c (kN/m^2)	Dry unit weight γ_{dry} (kN/m^3)
Stat.1b	−10.3	16.1
Stat.2b	−41.3	17.0
Stat.3b	−68.9	16.2

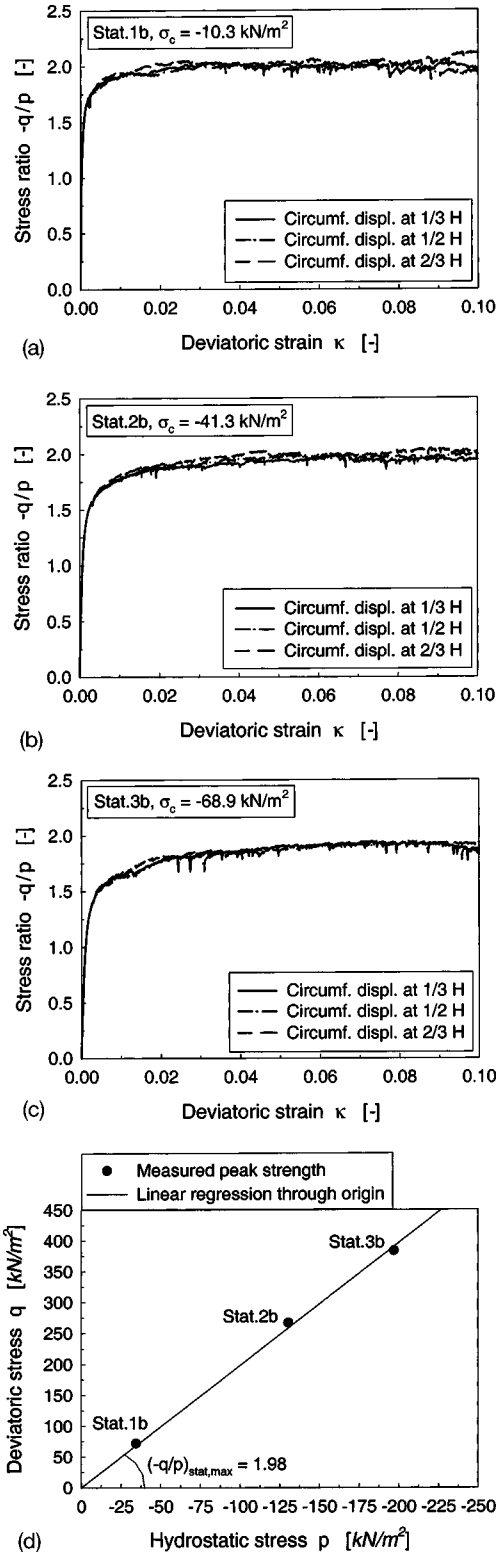

Fig. 9. Static response of ballast material. Stress and strain parameters determined with the measurements at $H/3$, $H/2$, and $2H/3$: (a) variation of stress ratio $-q/p$ with total deviatoric strain κ, where the confining pressure $\sigma_c = -10.3$ kN/m^2; (b) variation of stress ratio $-q/p$ with total deviatoric strain κ, where the confining pressure $\sigma_c = -41.3$ kN/m^2; (c) variation of stress ratio $-q/p$ with total deviatoric strain κ, where the confining pressure $\sigma_c = -68.9$ kN/m^2; and (d) comparison of measured values of peak strength in the $p-q$ plane with corresponding linear regression line

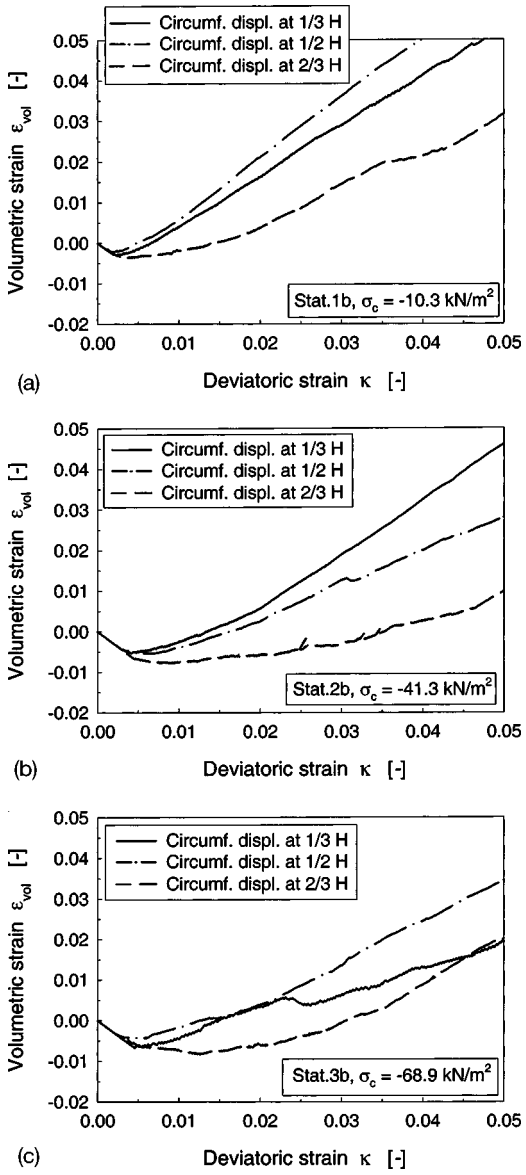

Fig. 10. Static response of ballast material. Stress and strain parameters determined with circumferential displacement measurements at $H/3$, $H/2$ and $2H/3$. Variation of total volumetric strain ε_{vol} with total deviatoric strain κ: (a) response for a confining pressure $\sigma_c = -10.3$ kN/m^2; (b) response for a confining pressure $\sigma_c = -41.3$ kN/m^2; and (c) response for a confining pressure $\sigma_c = -68.9$ kN/m^2.

dilation. As for the subballast material, at increasing confining pressure the amount of dilation decreases. It is seen in each figure that the three deformation curves start to diverge from each other when the deformation grows. This corresponds to the emergence of inhomogeneous failure modes, which are triggered because of the slender geometry of the ballast specimen (i.e., the aspect ratio of the ballast specimen is $H/D = 2.53$).

Results from Cyclic Tests

The cyclic loading tests on the ballast material were performed in a load-controlled fashion at a frequency of 5 Hz, where the specimen response was periodically registered during 1,000,000 load cycles. In Table 5, the characteristics for the cyclic tests are pre-

Table 5. Characteristics of One Million Load Cycle Tests on Ballast Material

Test	Confining pressure σ_c (kN/m^2)	Relative cyclic stress n (−)	Dry unit weight γ_{dry} (kN/m^3)
Cyc.1b	−41.3	0.510	16.3
Cyc.2b	−41.3	0.822	16.3
Cyc.3b	−41.3	0.964	16.6
Cyc.4b	−41.3	0.979	16.6
Cyc.5b	−68.9	0.508	16.5
Cyc.6b	−68.9	0.817	16.8
Cyc. 7b	−68.9	0.958	16.6
Cyc.8b	−68.9	0.973	16.7

sented. It is emphasised that the relative cyclic stress n, as defined by Eq. (7), here relates to a static failure level of $(-q/p)_{stat,max}=1.98$, see Fig. 9(d).

In Figs. 11(a and b), the cyclic evolution of the deviatoric strain has been sketched for the two confining pressures selected. The stress and strain parameters used in this graphical presentation correspond to the average of the circumferential displacement measurements at $H/3$, $H/2$, and $2H/3$. The curves show a trend that is comparable to that measured for the subballast, see Figs. 6(a and b). It can be further observed that at lower cyclic stress levels, $n<0.82$, the permanent deformation rate at 1,000,000 load cycles has become negligibly small. In other words, the cyclic response has become (almost) elastic. This phenomenon is known as "shakedown."

The cyclic evolution of the volumetric strain, depicted in Figs. 11(c and d), shows that the ballast material is less susceptible to compaction than the subballast material, see Figs. 6(c and d). As explained before, the low compaction susceptibility stems from the uniform particle gradation of the ballast material. At stress levels close to failure, the volumetric strain rate is slightly positive at the initial loading stage. At about 1,000 load cycles, the dilation changes into compaction, after which the compaction level increases more or less linearly with the logarithm of the number of load cycles. During this stage, at relatively high stress levels, $0.96<n<1$, the permanent volumetric strain is larger than the total volumetric strain, as indicated by the sign of the (compressive) elastic volumetric strain being opposite to the sign of the (dilative) total and permanent volumetric strains. Note that in the beginning of the cyclic loading process this is not the case, due to the initial settling of the circumferential strain device. More specifically, at the onset of a loading process with a relatively high cyclic stress level, the circumferential displacement device starts slipping along some of the (coarse) grains at the specimen boundary before surrounding the ballast specimen in a stable manner. Figs. 11(c and d) illustrate that this settling effect takes place over approximately the first ten load cycles, causing the values of the elastic volumetric strain in this range to be erroneous.

In general, material compaction may be the result of particle rearrangement, particle crushing, or a combination of both mechanisms. Sieving procedures conducted after the tests were finished only revealed a small amount of particle breakage, which suggests that material compaction is driven here mainly by particle rearrangement. This finding is supported by additional static oedometer tests (Suiker 1999), which showed that for the current ballast material the hydrostatic stress at which particle crushing is

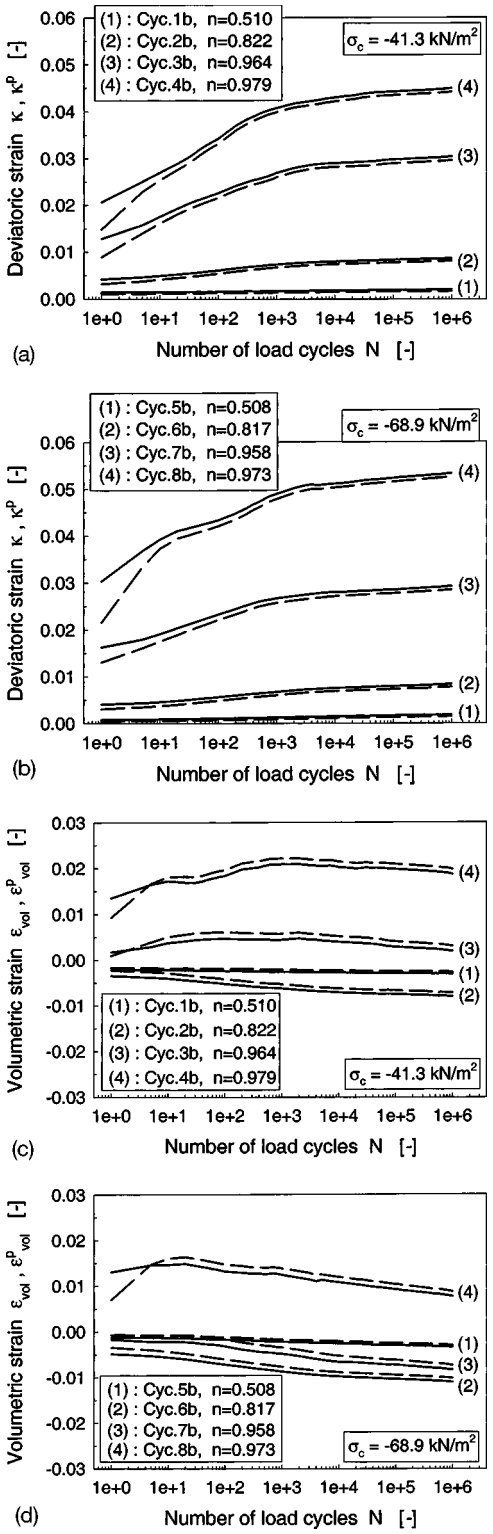

Fig. 11. Cyclic response of ballast material for various stress levels n: (a) increase of total deviatoric strain κ (solid line) and permanent deviatoric strain κ^p (dashed line) with load cycles N, for a confining pressure $\sigma_c=-41.3$ kN/m^2; (b) increase of total deviatoric strain κ (solid line) and permanent deviatoric strain κ^p (dashed line) with load cycles N, for a confining pressure $\sigma_c=-68.9$ kN/m^2; (c) variation of total volumetric strain ε_{vol} (solid line) and permanent volumetric strain ε^p_{vol} (dashed line) with load cycles N, for a confining pressure $\sigma_c=-41.3$ kN/m^2; and (d) variation of total volumetric strain ε_{vol} (solid line) and permanent volumetric strain ε^p_{vol} (dashed line) with load cycles N, for a confining pressure $\sigma_c=-68.9$ kN/m^2

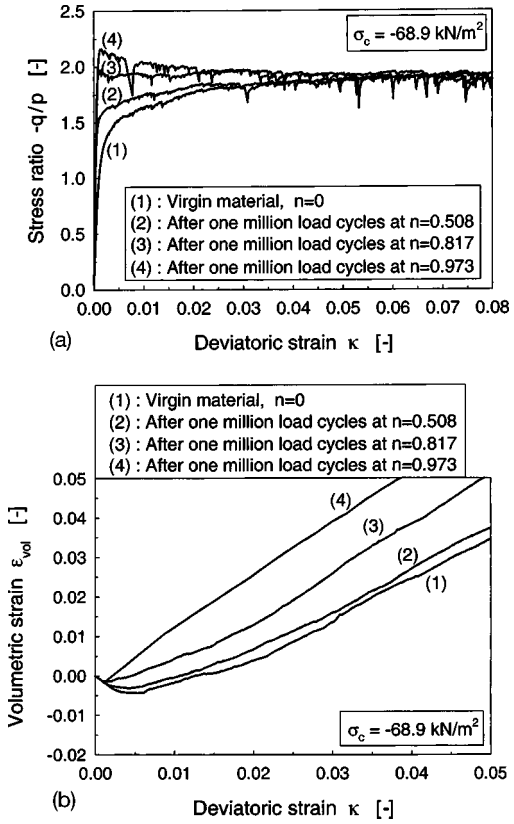

Fig. 12. Static response of ballast material after preloading at various cyclic stress levels n: (a) variation of stress ratio $-q/p$ with total deviatoric strain κ, where the confining pressure $\sigma_c=-68.9$ kN/m^2, and (b) variation of total volumetric strain ε_{vol} with total deviatoric strain κ, where the confining pressure $\sigma_c=-68.9$ kN/m^2

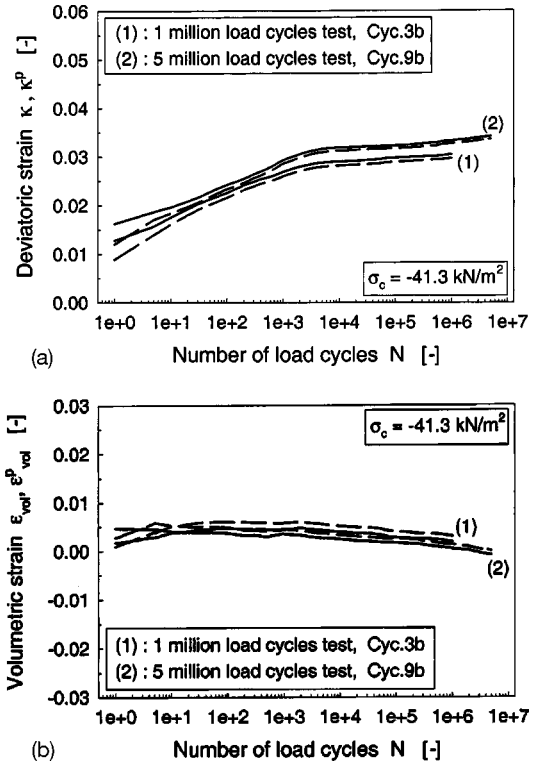

Fig. 13. Cyclic response of ballast material. Representation of test repeatability and response characteristics up to 5,000,000 load cycles: (a) increase of total deviatoric strain κ (solid line) and permanent deviatoric strain κ^p (dashed line) with load cycles N. The confining pressure $\sigma_c=-41.3$ kN/m^2. (b) Variation of total volumetric strain ε_{vol} (solid line) and permanent volumetric strain ε_{vol}^p (dashed line) with load cycles N. The confining pressure $\sigma_c=-41.3$ kN/m^2.

initiated is about $p\approx-350$ kN/m^2. This value is considerably higher than the maximum hydrostatic pressure used in the triaxial tests: $p=-193$ kN/m^2, see Fig. 9(d).

Static Failure after Cyclic Loading

The postcyclic failure behavior of the ballast is illustrated by the stress-strain curves in Fig. 12(a) and the deformation curves in Fig. 12(b). As for the subballast material, the cyclic loading process increases the peak strength, the stiffness, and the quasi-static dilation of the ballast. However, the increase in peak strength is less pronounced than for the subballast material; the peak strength obtained after cyclic loading at $n=0.973$ is only 9% higher than the peak strength of the virgin ballast material ($n=0$). This relates to an increase of the Mohr–Coulomb friction angle from $\phi_{stat,max}=48°$ ($n=0$) to $\phi_{stat,max}=53°$ ($n=0.973$). The small increase in peak strength can be ascribed to the low compaction susceptibility of the ballast. In addition, for cyclic stress levels close to failure, $0.96<n<1$, the ballast dilates before compacting, see Figs. 11(c and d); note that the low compaction susceptibility of the ballast causes the initial dilation at high stress levels to be larger than for the subballast, see Figs. 6(c and d).

The low compaction susceptibility is also the reason for the relative stiffness increase of the ballast material being smaller than that of the subballast material. More specifically, the virgin ballast material ($n=0$) has a secant shear modulus of $\mu^s_{-q/p=1.0}=33$ MPa for a stress ratio $-q/p=1.0$, whereas, for all cyclic stress levels considered, after the application of 1,000,000 load cycles the secant shear modulus of the ballast has become approximately equal to $\mu^s_{-q/p=1.0}\approx115$ MPa. This corresponds to a stiffness increase of a factor of 3.5. At large deviatoric strain, the postcyclic stress-strain curves in Fig. 12(a) closely resemble, and approach a constant shear strength.

Test Repeatability and Response to 5,000,000 Load Cycles

The properties of the 5,000,000 load cycles test are presented in Table 6. To analyze the test repeatability, the results are compared to those of Test *Cyc.3b*, of which the test characteristics are given in Table 5. Apparently, the cyclic evolution of the deviatoric strain [Fig. 13(a)], as well as the cyclic evolution of the volumetric strain [Fig. 13(b)], are in reasonable agreement. The discrepancies in the responses are believed to be due to differences in stress level and initial material density. Similar to the subballast material, the permanent deformations produced after 1,000,000 load cycles are very small.

Table 6. Characteristics of Five Million Load Cycle Test on Ballast Material

Test	Confining pressure σ_c (kN/m^2)	Relative cyclic stress n (−)	Dry unit weight γ_{dry} (kN/m^3)
Cyc.9b	−41.3	0.956	16.3

Concluding Remarks

The elastoplastic behavior of a ballast and subballast material has been explored by means of static and cyclic triaxial tests. The cyclic triaxial tests were carried out to provide insight into the deformation characteristics of these railway substructure materials under a large number of passing train wheels. The purpose of the static tests was to identify the maximum stress level that could be used in the cyclic tests, and to assess the strength and stiffness increase produced by the cyclic loading process.

It has been shown that the application of cyclic loading can lead to a considerably increase in material strength and stiffness. From the viewpoint of track stabilization, track maintenance procedures should aim at preserving consolidated granular substructures as much as possible. In this respect, stoneblowing is preferable to tamping. While stoneblowing only adds granular material to the ballast surface to smoothen the track, during tamping the track is smoothed by means of disturbing the ballast layer. The latter method thus reduces the compaction level of the ballast. Consequently, after a tamping operation has taken place, the rate of geometry deterioration usually is higher than before the tamping operation (Esveld 1989; Selig and Waters 1994).

For both the subballast and the ballast materials, the permanent deviatoric deformations generated under cyclic loading are strongly dependent on the stress ratio $(-q/p)_{\text{cyc}}$. In addition, the permanent volumetric deformation is governed by both the stress ratio $(-q/p)_{\text{cyc}}$ and the hydrostatic pressure p. A proper simulation of track deterioration thus requires adequate incorporation of these two stress effects into a cyclic densification model, see Suiker (2002) and Suiker and de Borst (2003).

References

Alva-Hurtado, J. E.D. (1980). "A methodology to predict the elastic and inelastic behavior of railroad ballast." Dissertation, Univ. of Massachusetts, Amherst.

Anderson, W. F., and Key, A. J. (2000). "Model testing of two-layer railway track ballast." *J. Geotech. Geoenviron. Eng.* 126(4), 317–323.

AREMA. (2002). "Sect. 2.4.4, Gradations." *Manual for railway engineering*.

Brown, S. F. (1974). "Repeated load testing of a granular material." *J. Geotech. Eng. Div., Am. Soc. Civ. Eng.*, 100(7), 825–841.

Esveld, C. (1989). *Modern railway track*, MRT Productions, Germany.

Frenkel, R. (2000). "Radial strain measurement device for triaxial testing." MS thesis, Dept. of Civil and Environmental Engineering, Univ. of Massachusetts, Amherst.

Galjaard, P. J., Paute, J. L., and Dawson, A. R. (1996). "Comparison and performance of repeated load triaxial test equipment for unbound granular materials." *Flexible pavements*, A. Gomes Correia, ed., A.A. Balkema, Rotterdam, The Netherlands.

Hjortnaes-Pedersen, A., and Molenkamp, F. (1982). "Accuracy and reproducibility of triaxial tests." In P. A. Vermeer, and H. J. Luger, eds., *Deformation and failure of granular materials*, A.A. Balkema, Rotterdam, The Netherlands, 391–401.

Indraratna, B., Ionescu, D., and Christie, H. D. (1998). "Shear behavior of railway ballast based on large-scale triaxial tests." *J. Geotech. Geoenviron. Eng.* 124(5), 439–449.

Lambe, T. W., and Whitman, R. V. (1969). *Soil mechanics*, Wiley, New York.

Lee, K. L., and Seed, H. B. (1967). "Drained strength characteristics of sands." *J. Soil Mech. Found. Div.*, 93, 117–141.

Raymond, G. P., and Davies, J. R. (1978). "Triaxial tests on dolomite railroad ballast." *J. Geotech. Eng. Div., Am. Soc. Civ. Eng.* 104(6), 737–751.

Selig, E. T., and Waters, J. M. (1994). *Track geotechnology and substructure management*., Thomas Telford, London.

Selig, E. T., Yoo, T. S., Adegoke, C. W., and Stewart, H. E. (1981). "Status report-Ballast experiments, Intermediate (175 mgt), Substructure stress and strain data." *Tech. Rep. FAST/TTC/TM-81/03*, Univ. of Massachusetts, for U.S. DOT Transportation Systems Center, Cambridge, Mass.

Stewart, H. E. (1982). "The prediction of track performance under dynamic traffic loading." Dissertation, Univ. of Massachusetts, Amherst.

Suiker, A. S. J. (1999). "Static and cyclic loading experiments on noncohesive granular materials." *Tech. Rep. 1-99-DUT-1*, Dept. of Civil Engineering, Delft Univ. of Technology, Delft, The Netherlands.

Suiker, A. S. J. (2002). "The mechanical behaviour of ballasted railway tracks." Dissertation, Delft Univ. of Technology, Delft, The Netherlands. pdf-format available at http://www.library.tudelft.nl/dissertations/

Suiker, A. S. J., and de Borst, R. (2003). "A numerical model for the cyclic deterioration of railway tracks." *Int. J. Numer. Methods Eng.* 57, 441–470.

van der Giessen, E., and de Borst, R. (1998). "Introduction to material instabilities in solids." *Material instabilities in solids*, R. de Borst, and E. van der Giessen, eds., Wiley, Chichester.

Vardoulakis, I., and Sulem, J. (1995). *Bifurcation analysis in geomechanics*, Blackie, London.

Wood, D. M. (1990). *Soil behaviour and critical state soil mechanics*, Cambridge University Press, Cambridge, U.K.